Geoscientific
Model Development

A lumped species approach for the simulation of secondary organic aerosol production from intermediate-volatility organic compounds (IVOCs): application to road transport in PMCAMx-iv (v1.0)

Stella E. I. Manavi[1,2] and Spyros N. Pandis[1,2]

[1]Department of Chemical Engineering, University of Patras, Patras, 26540, Greece
[2]Institute of Chemical Engineering Sciences, Foundation for Research and Technology – Hellas, Patras, 26540, Greece

Correspondence: Spyros N. Pandis (spyros@chemeng.upatras.gr)

Abstract. Secondary organic aerosol (SOA) is formed in the atmosphere through the oxidation and condensation of organic compounds. Intermediate-volatility compounds (IVOCs), compounds with effective saturation concentration (C^*) at 298 K between 10^3 and 10^6 µg m^{-3}, have high SOA yields and can be important SOA precursors. The first efforts to simulate IVOCs in chemical transport models (CTMs) used the volatility basis set (VBS), a highly parametrized scheme that oversimplifies their chemistry. In this work we propose a more detailed approach for simulating IVOCs in CTMs, treating them as lumped species that retain their chemical characteristics. Specifically, we introduce four new lumped species representing large alkanes, two lumped species representing polyaromatic hydrocarbons (PAHs) and one species representing large aromatics, all in the IVOC range. We estimate IVOC emissions from road transport using existing estimates of volatile organic compound (VOC) emissions and emission factors of individual IVOCs from experimental studies. Over the European domain, for the simulated period of May 2008, estimated IVOC emissions from road transport were about 21 Mmol d^{-1}, a factor of 8 higher than emissions used in previous VBS applications. The IVOC emissions from diesel vehicles were significantly higher than those from gasoline ones. SOA yields under low-NO$_x$ and high-NO$_x$ conditions for the lumped IVOC species were estimated based on recent smog chamber studies. Large cyclic alkane compounds have both high yields and high emissions, making them an important, yet understudied, class of IVOCs.

1 Introduction

Intermediate-volatility organic compounds (IVOCs) have effective saturation concentration (C^*) between 10^3 and 10^6 µg m^{-3} at 298 K, and they are emitted as gases in the atmosphere (Donahue et al., 2006; Robinson et al., 2007). Despite their lower emissions compared to volatile organic compounds (VOCs), IVOCs can be important secondary organic aerosol (SOA) precursors due to their high SOA yields (Tkacik et al., 2012; Docherty et al., 2021). IVOC sources include diesel and gasoline vehicles (Schauer et al., 1999; Gordon et al., 2014; Zhao et al., 2014, 2015, 2016; Drozd et al., 2019; Tang et al., 2021), biomass burning (Schauer et al., 2001; Ciarelli et al., 2017; Hatch et al., 2017; Qian et al., 2021), ships (Huang et al., 2018; Lou et al., 2019; Su et al., 2020) and consumer products (Li et al., 2018; Seltzer et al., 2021). Hydrocarbons, such as intermediate-length C$_{12}$–C$_{22}$ alkanes (linear, branched and cyclic), small polycyclic aromatic hydrocarbons (PAHs) and intermediate length aromatics, have been identified in the exhaust of fossil fuel combustion engines, while oxygenated IVOCs, such as phenols (both substituted and unsubstituted) and furans (both substituted and unsubstituted), have been detected in the emissions of biomass burning and consumer products. There are hundreds of isomers of these relatively large compounds, so they are difficult to separate by traditional gas-chromatography-based techniques. In gas chromatograms the majority of the emitted IVOCs usually appears as an unresolved complex mixture (UCM) of co-eluting compounds (Schauer et al., 1999, 2001). As a result, their identification and quantification are challenging, and their emissions are not well constrained.

Usually, their emissions are estimated based on other known emissions from the same source. Robinson et al. (2007) assumed that the IVOC emissions in the United States are 1.5 times the non-volatile primary organic aerosol (POA) emissions. This 1.5 factor is a zeroth-order assumption based on chassis dynamometer tailpipe measurements of diesel emissions (Schauer et al., 1999). A number of follow-up studies used the same approach and the same or different ratios to POA (Murphy and Pandis, 2009; Koo et al., 2014; Woody et al., 2016). Other studies proposed the scaling of the IVOC emissions to the corresponding VOC emissions (Jathar et al., 2013, 2014, 2017; Akherati et al., 2019). Most of these previous efforts have assumed the same IVOC / POA or IVOC / VOC ratio for the emissions of all sources. However, it is clear that source-specific scaling factors are needed (Lu et al., 2018).

Until recently, the role of IVOCs in the formation of SOA was neglected as the atmospheric concentrations of IVOCs are much lower than those of VOCs. However, IVOCs due to their size and low volatility have significantly higher SOA yields than VOCs (Lim and Ziemann, 2009; Presto et al., 2010; Tkacik et al., 2012; Docherty et al., 2021). For example, the measured SOA yields of linear alkanes increase with increasing number of carbons (Lim and Ziemann, 2009; Tkacik et al., 2012; Aumont et al., 2012). Besides carbon number, alkane structure also plays an important role in SOA formation. For an alkane with a given number of carbons, the cyclic isomers have higher SOA yields compared to the linear compounds, whereas the branched isomers have lower yields (Lim and Ziemann, 2009; Tkacik et al., 2012; Aumont et al., 2013). Smog chamber studies with other compounds in the IVOC range, such as PAHs, have also reported high SOA yields (Chan et al., 2009; Shakya and Griffin, 2010; Kleindienst et al., 2012; Chen et al., 2016).

The first efforts to simulate IVOCs in chemical transport models (CTMs) used four volatility bins (10^3–$10^6 \mu g \, m^{-3}$) of the volatility basis set (VBS) to describe their emissions and a highly parametrized chemical scheme (gas-phase reactions with OH lead to the reduction of the volatility of the products by one or more bins compared to the precursor) to simulate the IVOC oxidation (Robinson et al., 2007; Murphy and Pandis, 2009; Tsimpidi et al., 2010). In these schemes, each volatility bin includes thousands of individual IVOCs that are assumed to follow the same oxidation path, even if they have quite different chemical structure. This oversimplification of the chemistry of the IVOCs using the VBS is clearly a weakness. Besides IVOCs, the VBS framework also simulates SOA formation from compounds with lower C^*, such as semi-volatile organic compounds (SVOCs) (compounds with C^* between 1 and $100 \mu g \, m^{-3}$). A few studies used surrogate species such as naphthalene (Pye and Seinfeld, 2010) or n-pentadecane (Ots et al., 2016) to represent all IVOCs. This allowed them to improve the description of the corresponding chemical reactions but oversimplified the wide range of IVOCs present in the atmosphere.

Jathar et al. (2014) showed that the representation of IVOCs from combustion sources with three source-specific surrogate species resulted in improved SOA production predictions.

Zhao et al. (2014) measured the concentrations of both speciated and unspeciated atmospheric IVOCs in Pasadena, CA during the California at the Nexus of Air Quality and Climate Change (CalNex) study. They separated the UCM mass into 11 bins (B_{12}–B_{22}) which correspond to the retention times of 11 n-alkanes (C_{12}–C_{22}). The IVOC UCM mass within each retention bin was further separated into two chemical groups, one representing unspeciated branched alkanes and one representing the remaining UCM, which is likely a mixture of coeluting cyclic compounds (unspeciated cyclic compounds). These retention time bins B_i will also be used in the rest of our work for linking the UCM mass with the lumped IVOCs. Using the same approach in laboratory emissions studies, Zhao et al. (2015, 2016) estimated the emission factors (EFs) of 79 IVOCs emitted from on-road and off-road diesel and gasoline vehicles. Lu et al. (2020) simulated the SOA formation during the oxidation of these 79 IVOCs over the United States, by lumping them into six species based on their volatility and their chemical characteristics. The model of Lu et al. (2020) included IVOCs emitted from mobile sources and utilized a semi-empirical SOA parametrization based on the experimental work of Zhao et al. (2015, 2016). Implementing a lumped species approach, as the one proposed by Lu et al. (2020), improves the representation of the chemical complexity and variability of atmospheric IVOCs. However, it should be noted that the lumped IVOCs in the Lu et al. (2020) approach were still characterized by their volatility, and they were chemically separated as aromatic and alkane species. Qin et al. (2021) and Pennington et al. (2021) extended the model of Lu et al. (2020) to include IVOCs emitted from consumer products. The emission factors reported by Zhao et al. (2015, 2016) have also been used to estimate the IVOC VBS emissions from diesel and gasoline vehicles in the Po Valley (northern Italy) (Giani et al., 2019). Other studies have followed the Zhao et al. (2014) approach to estimate emissions both from on-road transport (Tang et al., 2021; Fang et al., 2021) and from various other sources such as non-road construction machinery (Qi et al., 2019), residential solid fuel combustion (Qian et al., 2021) and ship engines (Huang et al., 2018; Lou et al., 2019; Su et al., 2020). Li et al. (2019) conducted field measurements in the city of Shanghai in China and characterized IVOCs by using the approach of Zhao et al. (2014).

Improving the simulation of the formation of SOA from IVOCs (SOA-iv) in CTMs could reduce the gap between measured and predicted SOA (Pye and Seinfeld, 2010; Barsanti et al., 2013; Jathar et al., 2014; Ots et al., 2016; Zhao et al., 2016; Giani et al., 2019; Lu et al., 2020). In this work, we develop a new approach for simulating IVOCs in atmospheric CTMs, treating IVOCs as lumped species that retain their chemical characteristics (alkanes, alkenes,

aromatics, polyaromatics, etc.). Their atmospheric chemistry and resulting SOA formation is described similarly to that of the larger VOCs. Even though SVOCs can also be important SOA precursors, their chemical complexity together with the limited existing information about their gas-phase chemistry and SOA production prevents us from including them in the proposed scheme at this stage. The inclusion of the even more chemically complex low-volatility organic compounds (LVOCs) is even more challenging, so they are also treated using the VBS in the present work. The proposed lumping scheme, the source-specific emissions, the lumped chemical mechanism and SOA formation parametrization are described here. The implementation of the new IVOC approach in PMCAMx (the new version is called PMCAMx-iv), a three-dimensional CTM, and its evaluation is described in a subsequent publication. The proposed approach is general enough to be portable to other regional and global CTMs. A brief description of the model requirements for the implementation of the proposed IVOC approach can be found in the Supplement. In this work, the proposed IVOC scheme is applied to on-road transportation and more specifically to IVOCs emitted by diesel and gasoline vehicles following the studies of Zhao et al. (2015, 2016). IVOCs from other sources will be the topic of future work.
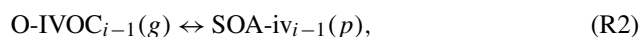
2   Methods

2.1   The SAPRC gas-phase mechanism

The gas-phase chemical mechanism employed in this application is based on a modified version of the SAPRC99 mechanism (Carter, 2010; Environ, 2013). Most of the VOCs are simulated in the SAPRC as lumped species. The criteria used to lump the individual VOCs are their chemical characteristics and their reaction rate constant with the hydroxyl radical (k_{OH}). The version of SARPC used as the starting point of this approach includes 237 reactions of 91 gases and 18 free radicals. Five lumped species represent alkanes (ALK1, ALK2, ALK3, ALK4, ALK5), two represent olefins (OLE1, OLE2), two represent aromatics (ARO1, ARO2), and there is also one monoterpene (TERP) and one sesquiterpenes species (SESQ). Information about the composition of the nine lumped VOC species within the modified version of SAPRC can be found in Table S1 in the Supplement.

2.2   The current VBS approach in PMCAMx

PMCAMx treats both primary and secondary organic species as chemically reactive using the VBS approach (Donahue at al., 2006). The VBS framework is also utilized by other CTMs to simulate SOA formation from SVOCs and IVOCs (Woody et al., 2015; Giani et al., 2019; Huang et al., 2021). In the current work, the default VBS scheme is utilized as a benchmark against which the proposed approach is compared. For these reasons, here we present a summary of

the default VBS approach, while detailed information about its implementation in models like PMCAMx is provided by Murphy and Pandis (2009) and Tsimpidi et al. (2010). In the original VBS approach, organic aerosol (OA) is discretized into nine logarithmically spaced bins characterized by their effective saturation concentration at 298 K (C^* equal to 0.01–$10^6 \, \mu g \, m^{-3}$). IVOCs occupy the four highest VBS bins (C^* equal to 10^3, 10^4, 10^5 and $10^6 \, \mu g \, m^{-3}$). They are emitted in the gas phase and can form SOA-iv as they react with the hydroxyl radical. The aging OH reactions have a reaction rate constant of $4 \times 10^{-11} \, cm^3 \, molecule^{-1} \, s^{-1}$. Each reaction reduces the volatility of the oxidized vapor product by 1 order of magnitude, and it increases the mass by 7.5 % to account for the added oxygen. The following reactions describe the SOA-iv formation in the VBS approach currently in use:

$$\text{IVOC}_i(g) + \text{OH} \rightarrow 1.075 \, \text{O-IVOC}_{i-1}(g) \qquad \text{(R1)}$$

$$\text{O-IVOC}_{i-1}(g) \leftrightarrow \text{SOA-iv}_{i-1}(p), \qquad \text{(R2)}$$

where i is the corresponding volatility bin, O-IVOC$_i$ the secondary gas-phase products from the oxidation of IVOCs and SOA-iv$_{i-1}$ the aerosol products from the oxidation of the IVOC precursors.

2.3   The new IVOC lumping scheme

In the new IVOC modeling scheme, seven new lumped species are added to the SAPRC mechanism to describe the IVOCs based on their chemical type and their reaction rate constant with the hydroxyl radical (k_{OH}). This is consistent with the approach that has been used to develop the rest of the SAPRC mechanism. Four species (ALK6, ALK7, ALK8, ALK9) are used to represent C_{12}–C_{22} alkanes. One lumped species (ARO3) is used to represent aromatics with carbon numbers from 11 to 22 and two species (PAH1, PAH2) to represent C_{10}–C_{17} PAHs. The seven new lumped species and their components, their k_{OH}, their molecular weight (MW) and their estimated saturation concentration (C^*) are depicted in Table 1.

The individual compounds lumped into the seven new species are based on the studies of Zhao et al. (2015, 2016). The unspeciated cyclic compounds in the B_{12}–B_{16} retention bins are dominated by aliphatic compounds in diesel engine emissions and by aromatic compounds when they are emitted by gasoline vehicles (Zhao et al., 2015, 2016). The new lumped alkanes contain speciated and unspeciated linear, branched and cyclic alkanes. ALK6 includes alkanes and other non-aromatic compounds that react only with the hydroxyl radical and have a k_{OH} between 1.3 and $1.8 \times 10^{-11} \, cm^3 \, molecule^{-1} \, s^{-1}$; this corresponds to linear alkanes with 12 to 14 carbons. ALK7 includes linear, cyclic and branched C_{15}–C_{17} alkanes that have a k_{OH} between 1.8 and $2.2 \times 10^{-11} \, cm^3 \, molecule^{-1} \, s^{-1}$. Speciated and unspeciated C_{18}–C_{20} alkanes with a k_{OH} between 2.2 and $2.6 \times 10^{-11} \, cm^3 \, molecule^{-1} \, s^{-1}$ are lumped into ALK8, whereas ALK9 includes alkanes and

Table 1. Characteristics of the new lumped IVOC species.

No. carbons	Compound names	Reaction rate constant with OH k_{OH} ($\times 10^{-11}$ cm^3 molecule^{-1} s^{-1})	Molecular weight MW (g mol^{-1})	Estimated saturation concentration C^* (µg m^{-3})
ALK6 (MW = 183 g mol^{-1}) Alkanes and other non-aromatic compounds that react only with OH (k_{OH}: 1.3–1.8 $\times 10^{-11}$ cm^{-3} molecule^{-1} s^{-1})				
12	Dodecane	1.3	170	1.8×10^6
13	Tridecane	1.5	184	7.3×10^5
14	Tetradecane	1.7	198	3.0×10^5
14	2,6,10-Trimethylundecane	1.7	198	1.4×10^6
12	Hexylcyclohexane	1.8	168	1.7×10^6
	Unspeciated b-alkanes B12	1.3	170	1.8×10^6
	Unspeciated b-alkanes B13	1.5	184	7.3×10^5
	Unspeciated b-alkanes B14	1.7	198	3.0×10^5
	Unspeciated cyclic alkanes B12	1.3	170	1.8×10^6
	Unspeciated cyclic alkanes B13	1.5	184	7.3×10^5
	Unspeciated cyclic alkanes B14	1.7	198	3.0×10^5
ALK7 (MW = 224 g mol^{-1}) Alkanes and other non-aromatic compounds that react only with OH (k_{OH}: 1.8–2.2 $\times 10^{-11}$ cm^{-3} molecule^{-1} s^{-1})				
15	Pentadecane	1.8	212	1.2×10^5
16	Hexadecane	2.0	226	4.9×10^4
17	Heptadecane	2.1	241	2.0×10^4
15	2,6,10-Trimethyldodecane	1.9	212	5.8×10^5
16	2,6,10-Trimethyltridecane	2.1	226	2.4×10^5
13	Heptylcyclohexane	1.9	182	7.1×10^5
14	Octylcyclohexane	2.1	196	3.0×10^5
15	Nonylcyclohexane	2.2	210	1.2×10^5
	Unspeciated b-alkanes B15	1.8	212	1.2×10^5
	Unspeciated b-alkanes B16	2.0	226	4.9×10^4
	Unspeciated b-alkanes B17	2.1	241	2.0×10^4
	Unspeciated cyclic alkanes B15	1.8	212	1.2×10^5
	Unspeciated cyclic alkanes B16	2.0	226	4.9×10^4
	Unspeciated cyclic alkanes B17	2.1	241	2.0×10^4
ALK8 (MW = 265 g mol^{-1}) Alkanes and other non-aromatic compounds that react only with OH (k_{OH}: 2.2–2.6 $\times 10^{-11}$ cm^{-3} molecule^{-1} s^{-1})				
18	Octadecane	2.2	255	8.1×10^3
19	Nonadecane	2.4	269	3.3×10^3
20	Eicosane	2.5	283	1.3×10^3
18	2,6,10-Trimethylpentadecane	2.3	255	4.1×10^4
19	Pristane	2.4	269	2.9×10^4
20	Phytane	2.6	283	1.2×10^4
16	Decylcyclohexane	2.3	224	5.2×10^4
17	Undecylcyclohexane	2.5	239	2.2×10^4
18	Dodecylcyclohexane	2.6	253	9.1×10^3
	Unspeciated b-alkanes B18	2.2	255	8.1×10^3
	Unspeciated b-alkanes B19	2.4	269	3.3×10^3
	Unspeciated b-alkanes B20	2.5	283	1.3×10^3
	Unspeciated cyclic alkanes B18	2.2	255	8.1×10^3
	Unspeciated cyclic alkanes B19	2.4	269	3.3×10^3
	Unspeciated cyclic alkanes B20	2.5	283	1.3×10^3

Table 1. Continued.

No. carbons	Compound names	Reaction rate constant with OH k_{OH} ($\times 10^{-11}$ cm^3 molecule^{-1} s^{-1})	Molecular weight MW (g mol^{-1})	Estimated saturation concentration C^* (µg m^{-3})
ALK9 (MW = 302 g mol^{-1}) Alkanes and other non-aromatic compounds that react only with OH ($k_{OH} > 2.6 \times 10^{-11}$ cm^{-3} molecule^{-1} s^{-1})				
21	Heneicosane	2.7	297	5.4×10^2
22	Docosane	2.8	311	2.1×10^2
19	Tridecylcyclohexane	2.8	267	3.8×10^3
20	Tetradecylcyclohexane	2.9	281	1.6×10^3
21	Pentadecylcyclohexane	3.0	295	6.4×10^2
22	Hexadecylcyclohexane	3.2	309	2.6×10^2
23	Heptadecylcyclohexane	3.3	323	1.1×10^2
	Unspeciated b-alkanes B21	2.7	297	5.4×10^2
	Unspeciated b-alkanes B22	2.8	311	2.1×10^2
	Unspeciated cyclic alkanes B21	2.7	297	5.4×10^2
	Unspeciated cyclic alkanes B22	2.8	311	2.1×10^2
ARO3 (MW = 188 g mol^{-1}) Larger aromatics				
11	Pentylbenzene	1.0	148	2.4×10^6
12	Hexylbenzene	1.2	162	1.0×10^6
13	Heptylbenzene	1.3	176	4.1×10^5
14	Octylbenzene	1.4	190	1.7×10^5
15	Nonylbenzene	1.6	204	6.9×10^4
16	Decylbenzene	1.7	218	2.8×10^4
17	Undecylbenzene	1.9	232	1.2×10^4
18	Dodecylbenzene	2.0	246	4.7×10^3
19	Tridecylbenzene	2.1	261	1.9×10^3
20	Tetradecylbenzene	2.3	275	7.7×10^2
22	Pentadecylbenzene	2.4	289	3.1×10^2
PAH1 (MW = 137 g mol^{-1}) Polycyclic aromatic hydrocarbons with $k_{OH} < 7 \times 10^{-11}$ cm^{-3} molecule^{-1} s^{-1}				
10	Naphthalene	1.6	128	1.8×10^8
11	2-Methylnaphthalene	4.9	142	7.1×10^7
11	1-Methylnaphthalene	4.1	142	7.1×10^7
12	C2-Naphthalene	6.0	156	3.5×10^7
13	Fluorene	1.6	166	1.3×10^6
14	Phenanthrene	3.2	178	1.1×10^8
15	C1-Phenanthrene	5.9	192	4.7×10^7
16	Fluoranthene	3.3	202	3.7×10^8
16	Pyrene	5.6	202	3.0×10^8
	Unspeciated aromatic compounds B12	1.6	128	1.8×10^8
	Unspeciated aromatic compounds B13	4.9	142	7.1×10^7
	Unspeciated aromatic compounds B14	6.0	156	3.5×10^7
PAH2 (MW = 175 g mol^{-1}) Polycyclic aromatic hydrocarbons with $k_{OH} > 7 \times 10^{-11}$ cm^{-3} molecule^{-1} s^{-1}				
12	Acenaphthylene	12.4	152	1.3×10^7
12	Acenaphthene	8.0	154	1.4×10^7
13	C3-Naphthalene	8.0	170	1.1×10^7
13	C4-Naphthalene	8.0	184	4.4×10^6
14	C1-Fluorene	8.0	180	5.1×10^5
14	Anthracene	17.8	178	1.1×10^8
16	C2-Phenanthrene/anthracene	8.0	192	4.7×10^7
17	C1-Fluoranthene/pyrene	13.1	202	3.0×10^8
	Unspeciated aromatic compounds B15	8.0	170	1.1×10^7
	Unspeciated aromatic compounds B16	8.0	184	4.4×10^6

other non-aromatic compounds with a k_{OH} greater than 2.6×10^{-11} cm^3 molecule^{-1} s^{-1}. The new aromatic species ARO3 contains speciated alkylbenzenes that are not explicitly represented in the original SAPRC mechanism. The new PAH species contain unsubstituted and substituted PAHs and unspeciated larger aromatic compounds. PAH1 includes PAH compounds, such as naphthalene and methylnaphthalene isomers that have k_{OH} smaller than 7×10^{-11} cm^3 molecule^{-1} s^{-1}. PAH2 includes PAH compounds, such as acenaphthylene and acenaphthene that have k_{OH} greater than 7×10^{-11} cm^3 molecule^{-1} s^{-1}.

In the original SAPRC mechanism, ALK5 represented larger alkanes and other non-aromatic compounds that react with the hydroxyl radical with a k_{OH} greater than 0.6×10^{-11} cm^3 molecule^{-1}s^{-1}. To avoid double counting in the new scheme, ALK5 now includes compounds with a k_{OH} between 0.6 and 1.3×10^{-11} cm^3 molecule^{-1} s^{-1}. In the revised ALK5, the largest compounds represented are undecane and its isomers. The aromatic compounds lumped into the ARO3, PAH1 and PAH2 were not represented in the original SAPRC mechanism, and thus no change is needed for the ARO2 species.

For the speciated individual compounds, the OH reaction rate constants are taken from the literature when available (Ananthula et al., 2006; Atkinson and Arey, 2003; Lee et al., 2003; Phousongphouang and Arey, 2002; Reisen and Arey, 2002; Kwok et al., 1997) or estimated using structure–reactivity relationships (Kwok and Atkinson, 1995; Kameda et al., 2013; Zhao et al., 2015) or extrapolated from similar compounds. For the OH reaction constants of the unspeciated alkanes, the approach of Zhao et al. (2014) was adopted. Specifically, for the unspeciated alkanes in the nth bin, Zhao et al. (2014) assumed that their k_{OH} is the same as the linear alkane with the same number of carbons as the number of the retention time bin, B_i. This assumption was used for estimating the values of both unspeciated branched and cyclic alkanes in each retention bin. For example, the unspeciated cyclic alkanes in the B_{13} bin were assumed to have an OH reaction rate constant equal to that of n-tridecane (C$_{13}$H$_{28}$). These assumed OH reaction rate constants are a lower bound as the branched and cyclic isomers of an n-alkane have higher rate constants compared to the linear n-alkane. The OH reaction rate constants of the unspeciated aromatic compounds in the B_{12}–B_{16} retention bins are assumed to be equal to those of naphthalene, methylnaphthalene, dimethyl naphthalene, trimethyl naphthalene and tetramethyl naphthalene respectively following the approach proposed by Zhao et al. (2016).

The MW of the speciated and unspeciated individual compounds is depicted together with the OH reaction rate constants of the compounds in Table 1. The MW of both unspeciated branched and cyclic alkanes in the nth retention time bin is assumed to be approximately equal to that of the corresponding linear n-alkane. This may result in a minor underestimation of the molecular weight of some of the branched or cyclic alkanes (Zhao et al., 2014). For the MW

of the unspeciated aromatic compounds lumped into the new PAH species, the MW values of naphthalene and methyl-naphthalene isomers are used as surrogates. The MW of the new lumped species is estimated as an emissions-weighted average of the MW of the individual compounds lumped into each species (Table 1).

The effective saturation concentration (C^*) of the individual compounds (Table 1) is mainly needed for comparisons with the VBS approach, and they are not an essential part of the proposed approach. For the speciated compounds, C^* was calculated as

$$C_i^* = \frac{\zeta_i \, 10^6 \, P_i^{vap} \, MW_i}{R \, T},\tag{1}$$

where C_i^* (in µg m^{-3}) is the effective saturation concentration for the individual compound i, ζ_i is its activity coefficient (assumed to be equal to unity for all the compounds), P_i^{vap} is its saturation vapor pressure, MW_i is its molecular weight, T is the temperature and R is the ideal gas constant. The Nannoolal et al. (2008) group contribution method was used to estimate the vapor pressure for each compound. In order to be able to compare the new lumped species with the IVOCs of the VBS approach, the few compounds with C^* below 10^3 µg m^{-3} are assumed to be in the 10^3 µg m^{-3} volatility bin, and the few compounds with C^* above 10^6 µg m^{-3} are placed in the 10^6 µg m^{-3} bin.

2.4 Estimating the road transport emissions of the new IVOC lumped species

The lack of explicit representation of IVOCs in most emission inventories necessitated the estimation of the new lumped IVOC emissions based on the emissions of other species that are traditionally included in inventories. While the VBS approach utilizes the non-volatile and non-reactive POA, the proposed scheme makes use of the total VOC emissions. The emissions of the individual IVOCs are estimated by combing source-specific emission factors (EFs) of the individual compounds with source-specific EFs of VOCs. The emission rates of the individual IVOC i from the source j ($E_{i,j}$ in g h^{-1}) is estimated as

$$E_{i,j} = \frac{EF_{i,j}}{EF_{VOC,j}} E_{VOC,j},\tag{2}$$

where $EF_{i,j}$ (g kg$_{fuel}^{-1}$) is the j source emission factor of the ith IVOC, $EF_{VOC,j}$ (g kg$_{fuel}^{-1}$) the source-specific emission factor of the total VOCs emitted from source j and $E_{VOC,j}$ (g h^{-1}) the emission rates of the total VOCs emitted by source j. The emissions of new lumped species emitted by each source are estimated by adding all the individual compound emissions:

$$EM_{k,j} = \sum_{i=1}^{n} E_{i,j},\tag{3}$$

where $EM_{k,j}$ ($g\,h^{-1}$) is the emission rate of the lumped species k, which contains n individual compounds, by source j.
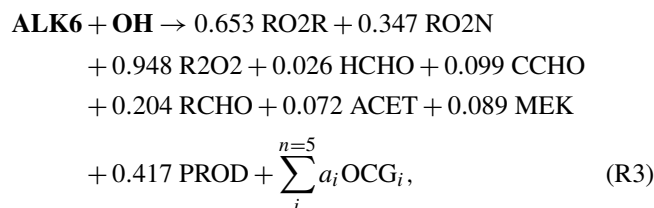
In this first application of the new scheme, we focus on IVOCs from diesel and gasoline vehicles, but the methodology described above can be easily used for other sources. The EFs of individual IVOCs from gasoline vehicles are based on the measurements of emissions of light-duty gasoline vehicles (LDGVs) by Zhao et al. (2016) in the United States. The application of these emission factors to European vehicles is a necessary assumption at this stage. The Zhao et al. (2016) study was based on a versatile fleet of gasoline vehicles under different driving cycles and the corresponding factors should be a zeroth approximation for European cars. The EFs of individual IVOCs from diesel vehicles used here are based on Zhao et al. (2015), who studied a combination of heavy-duty (HDDVs) and medium-duty diesel vehicles (MDDVs) used in the United States. Due to differences in regulations, in the United States, passenger cars with diesel engines only account for 3 % of the vehicles in circulation (Chambers and Schmitt, 2015), whereas in Europe, they account for 41.2 % (ACEA, 2017). For the purposes of this work, the EFs of individual IVOCs from diesel vehicles are assumed to be the same as those of the HDDVs in Zhao et al. (2015). This assumption probably leads to an overestimation of the diesel vehicle emissions, although previous studies have found that IVOC emissions depend more on fuel types rather than the type of vehicles (Cross et al., 2015; Lu et al., 2018). The emissions factors of the individual compounds from diesel and gasoline vehicles are summarized in Table S2. The EFs of the total emitted by the LDGVs and the HDDVs are taken respectively from the studies of Zhao et al. (2016, 2015). Finally, the total VOC emissions are based on the GEMS emissions inventory (Visschedijk et al., 2007).

2.5 Volatile, semi-volatile and low-volatility products from the oxidation of the new lumped IVOCs

Each of the seven new lumped IVOC species reacts with the hydroxyl radical and produces both volatile products, which remain in the gas phase, and less volatile products, which can partition to the aerosol phase, forming SOA-iv. In the new approach, the volatile products are simulated explicitly following the SAPRC framework, while the traditional VBS scheme is used to simulate the semi-volatile and low-volatility products of the IVOCs. Specifically, we assume that each of the seven newly added reactions with the hydroxyl radical contributes to the formation of the same five products with effective saturation concentrations of 0.1, 1, 10, 100 and 10^3 µg m^{-3} at 298 K. These products then partition between the gas and the particulate phase, forming SOA-iv. For the more volatile gas-phase oxidation products of the new reactions, like the produced ketones, and aldehydes as well as the various peroxy radicals, we have assumed that they are the same as the ones produced from the equivalent hydroxyl rad-
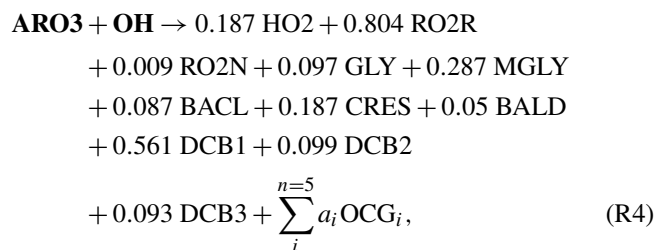
ical reactions of the larger lumped VOCs, particularly ALK5 and ARO2, which are already present in the SAPRC mechanism and have similar chemical characteristics. This simplification may lead to some errors of the yields of the volatile products of the reactions, but it is a good first step towards a more advanced representation of IVOC gas-phase chemistry.

The volatile products of the reactions of the four new lumped alkanes are assumed as a zeroth approximation to be the same as the ones produced by the reaction of ALK5 with the hydroxyl radical. As an example, the reaction of ALK6 with the hydroxyl radical is

$$
\begin{aligned}
\textbf{ALK6} + \textbf{OH} \rightarrow\; & 0.653\,\text{RO2R} + 0.347\,\text{RO2N} \\
& + 0.948\,\text{R2O2} + 0.026\,\text{HCHO} + 0.099\,\text{CCHO} \\
& + 0.204\,\text{RCHO} + 0.072\,\text{ACET} + 0.089\,\text{MEK} \\
& + 0.417\,\text{PROD} + \sum_{i}^{n=5} a_i \text{OCG}_i,
\end{aligned}
\tag{R3}
$$

where RO2R is the organic peroxy radical converting NO to NO_2 with HO_2 production, RO2N is the organic peroxy radical converting NO to organic nitrate, R2O2 is the organic peroxy radical converting NO to NO_2, HCHO is formaldehyde, CCHO is acetaldehyde, RCHO represents the higher aldehydes (based on propionaldehyde), ACET is acetone, MEK is methyl ethyl ketone, PROD represents other organic products, a_i is its NO_x-dependent mass-based yield and OCG_i is the ith oxygenated condensable lower-volatility product which can partition to the aerosol phase (all seven new lumped species contribute to the formation of the same five lower-volatility products). The reaction rate constant for Reaction (R3) is assumed conservatively to have the value of 1.4×10^4 ppm^{-1} min^{-1}, the same as the reaction of ALK5 with the hydroxyl radical. A similar reaction is used for the other new alkanes (ALK7–ALK9) (Table S3).

For the new aromatic and PAH species in the IVOC range, volatile products produced by the reaction with the hydroxyl radical are assumed as a zeroth approximation to be the same as the ones produced by the corresponding reaction of ARO2. As an example, the reaction of ARO3 with the hydroxyl radical is

$$
\begin{aligned}
\textbf{ARO3} + \textbf{OH} \rightarrow\; & 0.187\,\text{HO2} + 0.804\,\text{RO2R} \\
& + 0.009\,\text{RO2N} + 0.097\,\text{GLY} + 0.287\,\text{MGLY} \\
& + 0.087\,\text{BACL} + 0.187\,\text{CRES} + 0.05\,\text{BALD} \\
& + 0.561\,\text{DCB1} + 0.099\,\text{DCB2} \\
& + 0.093\,\text{DCB3} + \sum_{i}^{n=5} a_i \text{OCG}_i,
\end{aligned}
\tag{R4}
$$

where HO2 is the hydroperoxyl radical, GLY is glyoxal, MGLY is methylglyoxal, BACL is biacetyl, CRES is cresol, BALD is benzaldehyde and DCB1–DCB3 represent three different aromatic ring-opening dicarbonyl products. The reaction rate constant for Reaction (R4) is assumed to have

the value of $3.9 \times 10^4 \, \text{ppm}^{-1} \, \text{min}^{-1}$, the value of the k_{OH} for the reaction of ARO2 with the hydroxyl radical. Similar reactions are assumed for PAH1 and PAH2 (Table S3). In the proposed scheme, once the five condensable products are formed, they do not react any further with the hydroxyl radical. Conversely, the respective condensable gases that are formed from the oxidation reactions of anthropogenic VOCs do undergo multigenerational aging before they are allowed to partition to the aerosol phase. Both for consistency reasons and because the effect of multigenerational aging is worth investigating, multigenerational aging reactions have been included in the PMCAMx-iv (v1.0) code, but their reaction rate constants with the hydroxyl radical are set to zero. The effect of such reactions on the formation of SOA-iv in the new lumped species approach needs to be investigated in future work.

2.5.1 Estimating the yields for the new lumped IVOCs

For the simulation of the produced SOA-iv in the new scheme, it is necessary to estimate the NO_x-dependent mass-based yields (a_i) for each of the new lumped IVOC species. The first step of this process includes creating a database with smog chamber measurements of the SOA yields (Y) of the individual compounds at different organic aerosol concentrations (C_{OA}). Then, a fitting algorithm is used to estimate the yields for each of the studied precursors. The fitting algorithm estimates five mass-based coefficients (a_i), one for each of the five VBS products with C^* equal from 0.1 to $10^3 \, \mu\text{g m}^{-3}$. Moreover, when there are enough experimental data in the literature, different a_i's are estimated under high- and low-NO_x conditions. In the final step of this process, the five NO_x-dependent a_i's of the seven new lumped IVOC species are determined as a mass-emissions-weighted average of the estimated a_i's of the individual compounds lumped into each new species. In this study, as weights we utilize the mass-based fractions of the individual compound emissions coming from on-road diesel and gasoline vehicles (Table S2).

2.5.2 Fitting algorithm for estimating the mass-based yields

The fitting algorithm of Stanier et al. (2008) is utilized in this work to estimate the yields a_i for the individual compounds for fixed C_i^* corresponding to the VBS bins. Five SOA products with C_i^* at 298 K of 0.1, 1, 10, 100 and $10^3 \, \mu\text{g m}^{-3}$ were chosen. The algorithm estimates the values of the a_i's and of the effective vaporization enthalpy (ΔH) to reproduce the SOA measurements assuming the formation of a pseudo-ideal organic solution in the particulate phase. The algorithm tries to minimize the following objective function Q:

$$Q = \sum_i \left[Y_{i,\text{meas}} - Y_{i,\text{pred}}(a_i, \Delta H) \right]^2, \tag{4}$$

where $Y_{i,\text{meas}}$ is the measured aerosol SOA yields, and $Y_{i,\text{pred}}$ is the corresponding predicted yield for the choices of the parameters, using the VBS framework. The objective function Q is minimized using the *fmincon* MATLAB function (MathWorks, 2020). By minimizing the objective function, the optimal ΔH and a_i's are determined for the chosen C_i^* basis set. Factors such as the experimental conditions or the organic aerosol concentration range that the experiments cover influence the accuracy of the resulting parameters. Nevertheless, the chemical detail of the new lumped species approach could provide guidance to future experimental studies and allow them to focus on the more important IVOC families that are responsible for most of the SOA-iv production.

2.5.3 SOA yield measurements for individual IVOCs

The experimental studies used to estimate the individual compounds' mass-based yields with the algorithm described above are summarized in Table 2. For individual speciated alkanes in the IVOC range, smog chamber studies have focused on linear alkanes with available data covering only the high-NO_x conditions (Lim and Ziemann, 2009; Presto et al., 2010; Docherty et al., 2021). The studied linear alkanes include *n*-dodecane ($C_{12}H_{26}$), *n*-tridecane ($C_{13}H_{28}$) and *n*-tetradecane ($C_{14}H_{30}$) which are lumped into ALK6 and *n*-pentadecane ($C_{15}H_{32}$), *n*-hexadecane ($C_{16}H_{34}$) and *n*-heptadecane ($C_{17}H_{36}$) which are lumped into ALK7. The SOA production during the photo-oxidation of naphthalene, 1-methylnaphthalene and 2-methylnaphthalene has been investigated in a series of studies (Chan et al., 2009; Shakya and Griffin, 2010; Kleindienst et al., 2012; Chen et al., 2016). In these studies, the SOA yields of PAHs have been determined under both high- and low-NO_x conditions. For the individual compounds lumped into ALK8, ALK9, PAH2 and ARO3, there were no experimental data.

For the individual compounds with available data, the estimated mass-based yields are based on an assumed organic aerosol density, which is equal to $1 \, \text{g cm}^{-3}$ for the linear alkanes, $1.5 \, \text{g cm}^{-3}$ for naphthalene, $1.4 \, \text{g cm}^{-3}$ for 1-methylnaphthalene and $1.3 \, \text{g cm}^{-3}$ for 2-methylnaphthalene (Lim and Ziemann, 2009; Presto et al., 2010; Chan et al., 2009; Shakya and Griffin, 2010; Chen et al., 2016). For the new lumped alkanes (ALK6–ALK9), their estimated mass-based yields are based on an assumed aerosol density of $1 \, \text{g cm}^{-3}$, which is equal to that of the linear alkane SOA. For both PAH1 and PAH2, the assumed aerosol density is equal to $1.3 \, \text{g cm}^{-3}$, which corresponds to the aerosol density assumed for 2-methylnaphthalene. In the case of ARO3, the density assumed is $1 \, \text{g cm}^{-3}$, which is equal to that of ARO2 SOA.

IVOCs that have been studied so far represent only a small fraction of the total IVOC emissions; *n*-dodecane, *n*-tridecane and *n*-tetradecane compounds are only 5 % of the total ALK6 emissions, whereas *n*-pentadecane, *n*-hexadecane and *n*-heptadecane compounds represent

Table 2. Experimental smog chamber studies utilized in this work to estimate the mass-based stoichiometric yields of the individual IVOCs.

Compounds studied	Experimental conditions	Reference
n-Dodecane, n-tridecane, n-tetradecane, n-pentadecane, n-hexadecane, n-heptadecane	$T = 298$ K, exp. with RH < 1 % and exp. with RH > 15 %, high-NO$_x$ conditions, high-C_{OA} loadings	Lim and Ziemann (2009)
n-Dodecane, n-pentadecane, n-heptadecane	$T = 295$ K, RH < 20 %, high-NO$_x$ conditions	Presto et al. (2010)
n-Dodecane, n-tridecane, n-tetradecane	$T = 298$ K, RH varied, high-NO$_x$ conditions, no wall corrections	Docherty et al. (2021)
Naphthalene, 1-methylnaphthalene, 2-methylnaphthalene,	$T = 299$ K, RH from 5 % to 8 %, high- and low-NO$_x$ conditions	Chan et al. (2009)
Naphthalene, 1-methylnaphthalene, 2-methylnaphthalene	$T = 21$–25 °C, RH < 5 %, high- and low-NO$_x$ conditions	Shakya and Griffin (2010)
Naphthalene, 1-methylnaphthalene, 2-methylnaphthalene	$T = 298$ K, RH < 3 % high- and low-NO$_x$ conditions	Kleindienst et al. (2012)
Naphthalene, 1-methylnaphthalene, 2-methylnaphthalene	Dry conditions, high- and low-NO$_x$ conditions	Chen et al. (2016)

only 4 % of the total ALK7 emissions. Naphthalene, 1-methylnaphthalene and 2-methylnaphthalene compounds represent 19 % of the total PAH1 emissions. Several assumptions were applied to compensate for the missing information. In the future, as more experimental data become available, the assumptions described below can be relaxed.

In order to estimate the missing mass-based yields of speciated (linear, branched and cyclic) and unspeciated (branched and cyclic) alkanes, we adopted the approach of Zhao et al. (2014). For the missing speciated n-alkanes, we use the mass-based yields of n-heptadecane, the highest n-alkane for which there were data in the literature. This is a conservative assumption as the number of carbons of linear alkanes increases, and so does the aerosol mass fraction of the species (Lim and Ziemann, 2009; Presto et al., 2010; Aumont et al., 2012). For the missing speciated branched alkanes, we use the mass-based yields of the n-alkane with the same carbon minus the branching methyl groups. For example, the mass-based yields of 2,6,10-trimethyltridecane are assumed to be the same as these of n-tridecane. This provides a lower bound for our estimations (Lim and Ziemann, 2009; Tkacik et al., 2012; Aumont et al., 2012). For the missing speciated cyclic alkanes, we use the mass-based yields of the n-alkane with the same number of carbons. This is again a lower-bound estimate as experimental studies have

shown that for a given carbon number, the cyclic isomers have higher SOA yields compared to those of the linear alkanes (Lim and Ziemann, 2009; Tkacik et al., 2012). For the unspeciated branched alkanes, the mass-based yields are assumed to be the same as those of the linear n-alkane with an equal number of carbons minus 2. This assumption accounts for the effects of branching assuming that on average the unspeciated branched alkanes have four methyl branches. For the unspeciated cyclic alkanes, the mass-based yields are assumed to be the same as those of the linear n-alkane with an equal number of carbons. All the surrogate species utilized in each case can be found in Table S4.

The three PAHs, for which we have sufficient data to estimate the a_i yield parameters, are lumped into PAH1. For the unspeciated aromatic compounds in the B_{12} retention bin, the estimated naphthalene mass-based yields are used, following the approach of Zhao et al. (2016). In order to compensate for the missing data of the other compounds which are lumped into PAH1 and PAH2, the 2-methylnaphthalene mass-based yields are used (Table S4).

Finally, since there is no information about the SOA formation of the alkylbenzenes which are lumped into ARO3, we assumed that their mass-based yields were 20 % higher than those of ARO2, the lumped species that already exists in the mechanism and that represents aromatic compounds
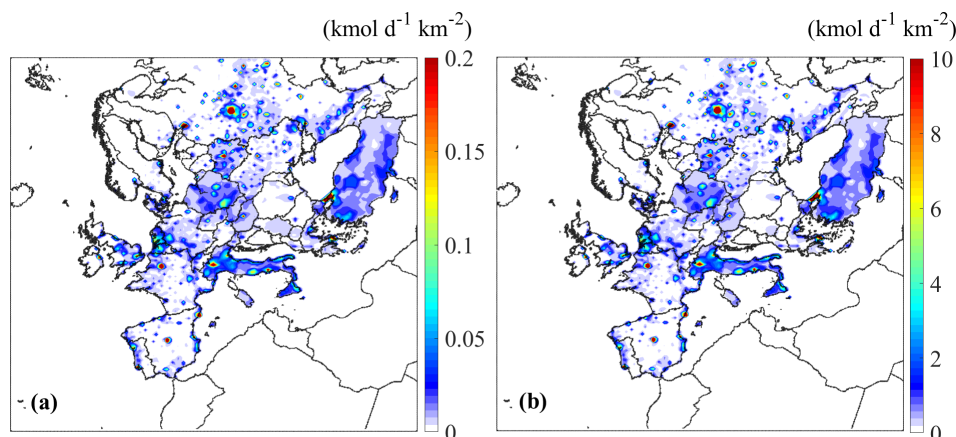
Figure 1. Estimated spatial distribution of the averaged emissions from on-road vehicles of **(a)** *n*-dodecane and **(b)** ALK6 for May 2008.
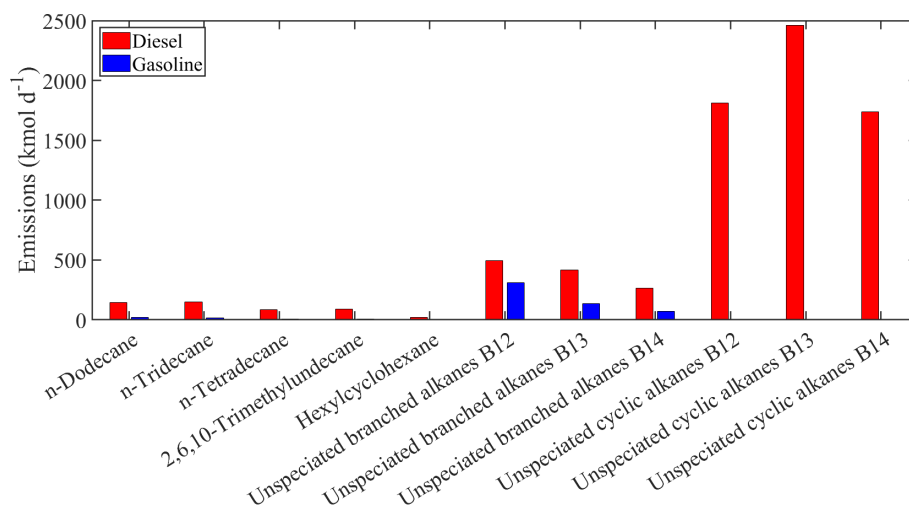

Figure 2. Estimated total gasoline and diesel emissions of the new individual compounds lumped into ALK6 for Europe.

(xylene and trimethyl benzene isomers). This assumption is a starting point for the new aromatic lumped species, and it will be evaluated in a subsequent publication.

3   Results and discussion

3.1   Estimated road transport emissions of IVOCs over Europe

The domain for the applications of this work covers a region of $5400 \times 5832\,\mathrm{km^2}$ over Europe, with a 36×36 grid resolution and 14 vertical layers of 6 km. The period used is that of May 2008 which corresponds to the European Aerosol Cloud Climate and Air Quality Interactions (EUCAARI) project intensive summer measurement campaign across Europe. Using the old VBS approach for estimating the IVOC emissions, for the simulated period, 17 % of the total anthropogenic IVOC emissions were attributed to on-road transport, of which 57 % was emitted by diesel vehicles and 21 %

by gasoline engines, and 22 % was due to non-exhaust emissions from vehicles.

The spatially and temporally resolved emissions from on-road diesel and gasoline vehicles of all the individual organic compounds depicted in Table 1 were estimated for the simulated period. The spatial and temporal distributions of the estimated emissions were determined based on the corresponding distributions of the VOCs emitted by the same sources in the GEMS inventory. As an example, the average emissions of *n*-dodecane and the corresponding emissions of ALK6, the lumped species that includes *n*-dodecane, are shown in Fig. 1. The estimated average transportation emissions of *n*-dodecane in different areas of Europe range from zero to $3.6\,\mathrm{mol\,d^{-1}\,km^{-2}}$. The highest emissions of *n*-dodecane are in major European cities, such as Athens, Paris, Madrid and London, and regionally in countries like Italy, Netherlands, UK and Poland. The temporal profile of the *n*-dodecane emissions in Paris (Fig. S1) indicates that, as expected, the on-road vehicle emissions peak each day during the morning
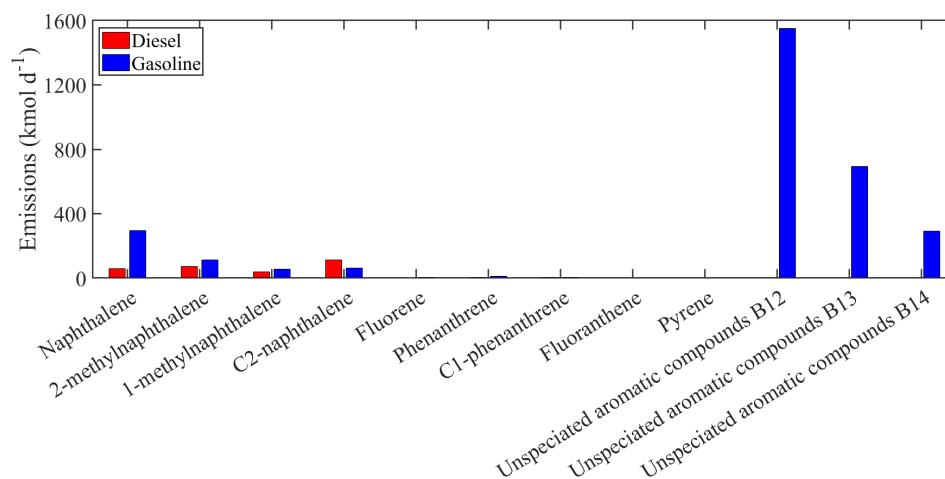
Figure 3. Estimated total gasoline and diesel emissions of the new individual compounds lumped into PAH1 for Europe.
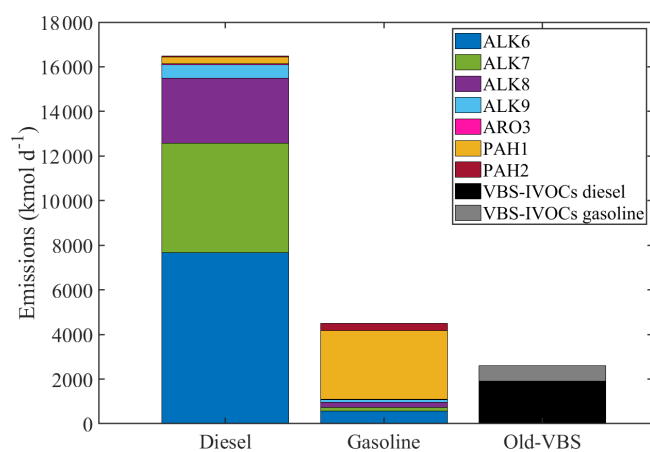

Figure 4. Total emissions from diesel and gasoline vehicles over Europe for May 2008 calculated using the new lumped species approach and using the old VBS approach (signified with grey and black).

and evening rush hours and are reduced during nighttime. For ALK6, our estimates of the average transport emissions range from zero to $182.3 \, \mathrm{mol \, d^{-1} \, km^{-2}}$. Again, the highest values of the ALK6 emissions are in major European cities. The transportation emissions of ALK6 are higher than those of n-dodecane, as n-dodecane corresponds to only 2 % of the ALK6 emissions (Table S2). The spatial distributions of the emissions of most IVOCs are quite similar to this example.

The estimated total on-road transportation emissions of the major individual compounds lumped into ALK6 are shown in Fig. 2. For both gasoline and diesel vehicles, the estimated emissions of the unspeciated alkanes are higher compared to the emissions of the other compounds lumped into ALK6. The unspeciated cyclic alkanes represent 73 % of the total emitted ALK6 mass, and the unspeciated branched alkanes are another 21 %. The three speciated linear alkanes (n-dodecane, n-tridecane and n-tetradecane) contribute 5 % and the other components less than 1 % each. The unspeciated cyclic alkanes in the B_{13} retention bin are the predominant components of the ALK6 diesel emissions. This is consistent with the measurements of Gentner et al. (2012), who reported that diesel emissions are dominated by aliphatic compounds with 13 to 18 carbons. The mass of the unspeciated cyclic compounds in the $B_{12}-B_{14}$ retention time bins, which appears to be missing from the gasoline ALK6 emissions (Fig. 2), is lumped into PAH1 as it is of aromatic nature (Zhao et al., 2016). The total estimated emissions of the individual compounds in PAH1 from both sources are shown in Fig. 3. Again, the unspeciated compounds are estimated to be the most important contributors to the total PAH1 emissions (75 % of the total PAH1), followed by naphthalene and the methylnaphthalene isomers (19 % of the total PAH1). The unspeciated cyclic aromatic compounds in the B_{12} retention bin have the highest total gasoline emissions, contributing 50 % of the total PAH1 emissions from gasoline vehicles. This is consistent with the measurements of Drozd et al. (2019), who reported that for gasoline vehicles, aromatic compounds in the B_{12} and B_{13} retention time bins have the highest IVOC emissions.

Using the new approach, the total IVOC emissions from diesel vehicles in Europe are approximately $16\,500 \, \mathrm{kmol \, d^{-1}}$ and from gasoline vehicles $4500 \, \mathrm{kmol \, d^{-1}}$ (Fig. 4). Previous studies have produced qualitatively consistent results with this estimation; diesel vehicles emit compounds predominantly in the IVOC range, while gasoline vehicles emit both VOCs and IVOCs (Gentner et al., 2012). The new total IVOCs emissions from on-road transportation are estimated to be 8 times higher than those calculated using the old VBS-approach. The total VBS emissions of IVOCs from diesel vehicles were $1950 \, \mathrm{kmol \, d^{-1}}$ and from gasoline vehicles $690 \, \mathrm{kmol \, d^{-1}}$. The higher IVOC emissions with the new approach compared to the VBS are consistent with the anal-
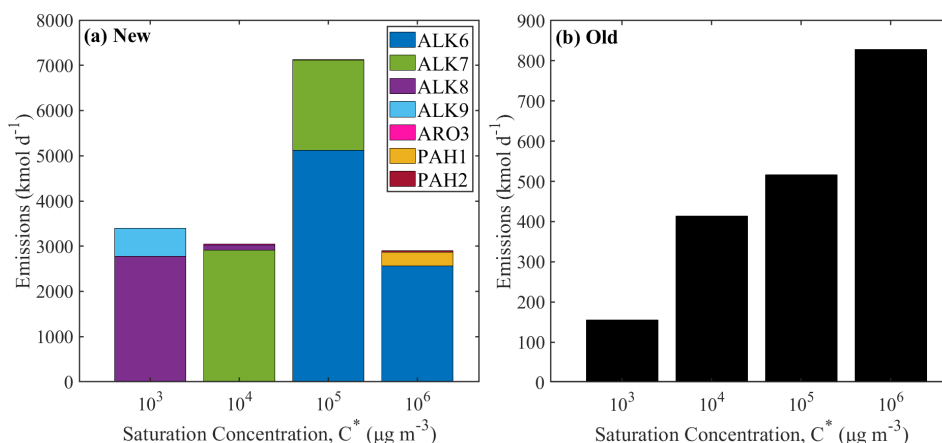
Figure 5. The volatility distribution of the IVOCs emissions from on-road diesel vehicles **(a)** using the new lumped species approach and **(b)** using the old VBS approach. Different axes are used for the two distributions.

ysis of Lu et al. (2018). These authors reported that estimating IVOC emissions by multiplying POA emissions with the 1.5 factor (current VBS approach) underestimates the IVOC emissions observed in experimental studies.

An advantage of the new lumped species' approach is that the IVOC emissions retain their chemical characteristics. We estimate that 98 % of the diesel IVOC emissions are large alkanes (ALK6–ALK9), and 76 % of the gasoline IVOC emissions are PAHs (PAH1 and PAH2) (Fig. 4). These are mainly unspeciated compounds (unspeciated branched and cyclic alkanes and unspeciated aromatic compounds). The most important contributor to the total IVOC emissions from diesel vehicles is ALK6 (7680 kmol d^{-1}), followed by ALK7 (4900 kmol d^{-1}) and ALK8 with total emissions of 2900 kmol d^{-1}. For gasoline vehicles, the highest emissions are again estimated to be those of PAH1 (3890 kmol d^{-1}), followed by ALK6, which contributes 13 % of the total new gasoline emissions. Aromatic and polyaromatic compounds are more prominent in gasoline emissions (Lu et al., 2018, 2020).

In order to better compare the new and old IVOC emissions, we have estimated the volatility distribution of the former. The volatility distribution of the emissions is quite different for the diesel emissions (Fig. 5). The traditionally assumed VBS diesel IVOC emissions are increasing as the volatility is increasing. Using the new lumped species approach, the IVOCs with $C^* = 10^5$ µg m^{-3} have the highest emissions, representing 43 % of the total. The new distribution resembles the measured volatility distribution of the unburned diesel fuel more closely (Lu et al., 2018; Drozd et al., 2019).

The old and new volatility distributions for the on-road gasoline vehicle are shown in Fig. 6. In this case, the highest emissions are those of the more volatile IVOCs with $C^* = 10^6$ µg m^{-3}. In the lumped species approach, 83 % of the total IVOCs emitted from gasoline vehicles have a satura-

tion concentration of 10^6 µg m^{-3}, while with the traditional VBS approach 43 % of the emissions have the same volatility. Once more, the volatility distribution of the new emissions more closely resembles that of the unburned fuel (Lu et al., 2018).

3.2 SOA yields for the new lumped IVOC species

3.2.1 Large alkane yields

The yields of the linear alkanes with 10 to 17 carbons were estimated based on experimental data and the fitting algorithm. The estimated parameters for all the speciated straight alkanes can be found in Table S5. As an example, the heptadecane yield as a function of the OA concentration is shown in Fig. 7. At room temperature, the estimated total SOA yield at OA concentration of 1 µg m^{-3} is 14 %, and at 10 µg m^{-3} it is 42.6 %. Please note that these yields include all the SOA components, while the yields in Table S5 are those of the individual products for both the gas and particulate phase. Organic aerosol concentrations of 1–10 µg m^{-3} are often encountered in the atmosphere, so heptadecane is a good SOA precursor under these conditions. The SOA yields as a function of the OA concentration of the other linear alkanes can be found in Fig. S7.

The estimated SOA yield parametrization of the new lumped IVOCs using the five-product VBS is summarized in Table 3. For the alkane lumped species, we have assumed that the values of a_i's are the same under both high- and low-NO$_x$ conditions. This is a necessary assumption due to lack of experimental measurements under low-NO$_x$ conditions. The estimated alkane yields increase with size from ALK6 to ALK9 (Fig. 8). At OA concentration of 1 µg m^{-3}, they range from 5.6 % for ALK6 and 12 % for ALK7 to 14 % for both ALK8 and ALK9. At an OA concentration of 10 µg m^{-3}, the SOA yields are 9.3 %, 34.2 %, 42 % and 43 % respectively. The predicted increase of the estimated yields with molecular
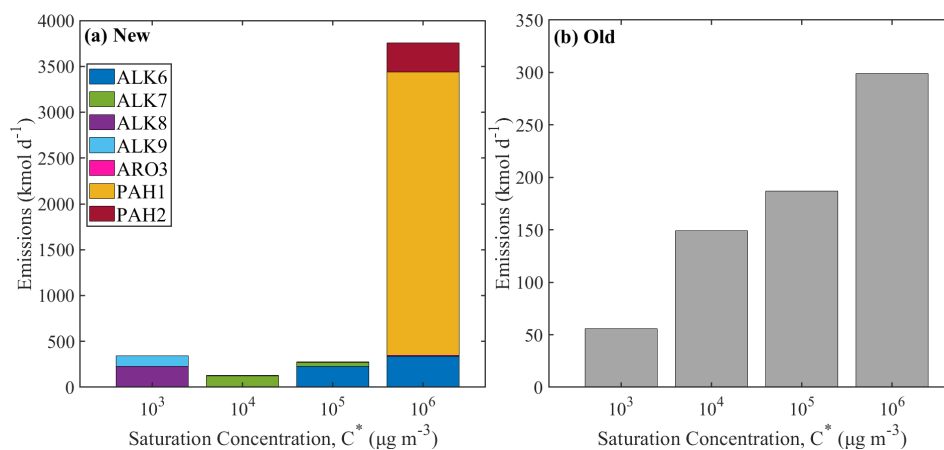
Figure 6. The volatility distribution of the IVOC emissions from on-road gasoline vehicles **(a)** using the new lumped species approach and **(b)** using the old VBS approach. Different axes are used for the two distributions.
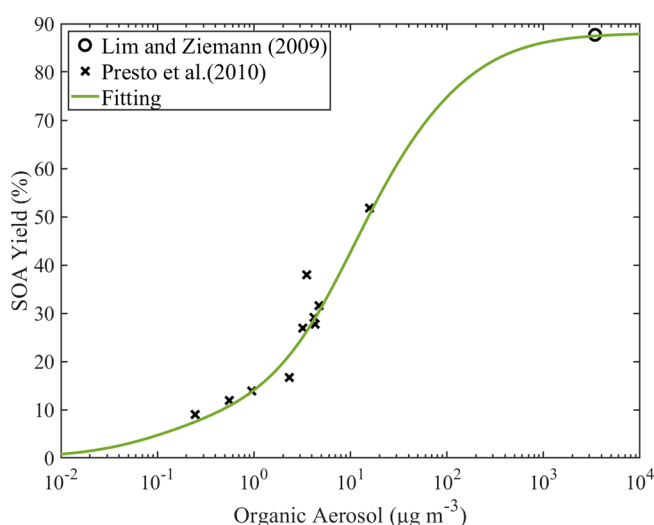

Figure 7. Estimated SOA yields of n-heptadecane under high-NO$_x$ conditions. The curve is generated using the estimated values of a_i (0.0771, 0.024, 0.6291, 0.1506 and 0). The data from the studies of Lim and Ziemann (2009) and Presto et al. (2010) that were used by the simplified algorithm are also shown.
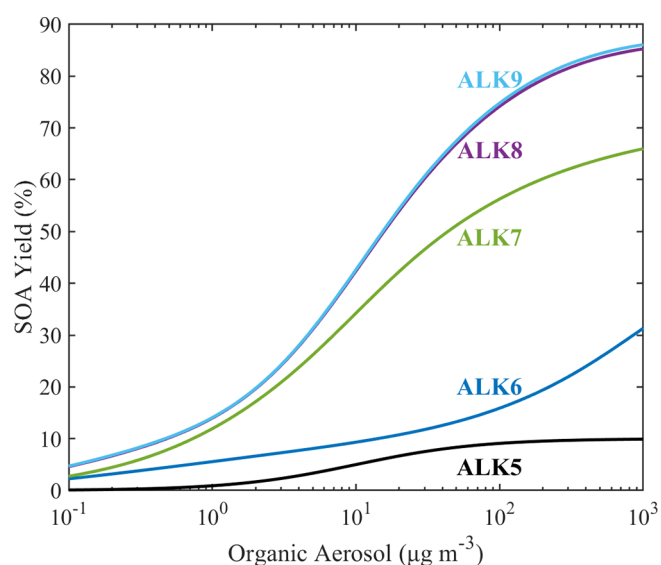
Figure 8. Estimated SOA yields of the new lumped alkane species under high-NO$_x$ conditions. The curves are generated using the SOA yield parametrization of Table 3.

size is in line with experiments that have shown that the SOA yields of cyclic and linear alkanes increase with carbon number (Lim and Ziemann, 2009; Presto et al., 2010; Tkacik et al., 2012). The estimated values of the organic aerosol yield of ALK8 and ALK9 are similar because they were based on the n-heptadecane yields, which is the highest linear alkane with experimental data available. This probably leads to an underestimation of the ALK9 yields.

All the SOA yields of the new alkane species are much higher that the yields of ALK5, which is the biggest lumped alkane species currently in SAPRC. According to the parametrization of Murphy and Pandis (2009), currently in PMCAMx, at OA of 1 µg m^{-3}, the SOA yield of ALK5

is 0.9 %, which is 6 times lower than that of ALK6 and 15 times lower than that of ALK9. At OA concentration of 10 µg m^{-3}, the SOA yield of ALK5 is 5 %, which is 2 times lower than that of ALK6 and 9 times lower than that of ALK9. It should be noted that the comparison between the new lumped IVOCs and the existing lumped VOCs (ALK5 and ARO2) is not used to assess the new approach but rather to emphasize the importance of IVOCs as SOA precursors.

3.2.2 PAH yields

Based on experimental data, the mass-based yields of naphthalene, 1-methylnaphthalene and 2-methylnaphthalene were estimated under both high- and low-NO$_x$ conditions (Ta-
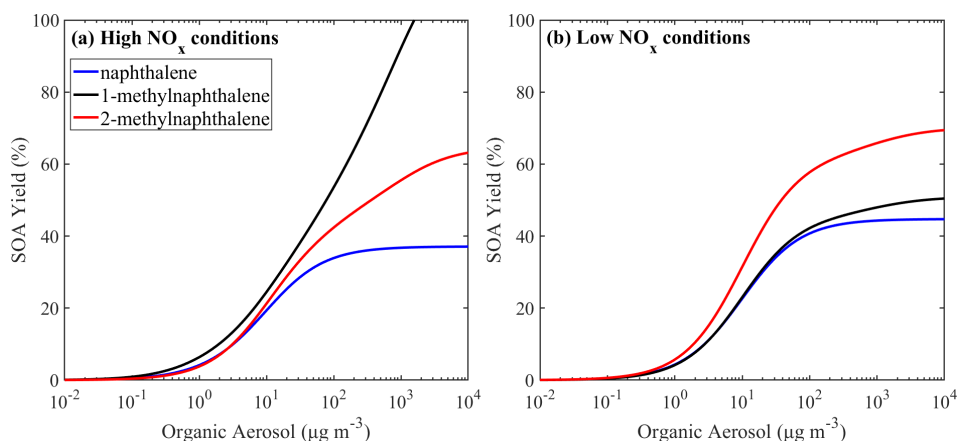
Figure 9. Estimated SOA yields of naphthalene, 1-methylnaphthalene and 2-methylnaphthalene under **(a)** high-NO$_x$ and **(b)** low-NO$_x$ conditions. The curves are generated using the estimated parameters of Table S5.

ble S5). The yields of these three compounds are shown in Fig. 9 as a function of the OA concentration. Under high-NO$_x$ conditions, the SOA yields of 1-methylnaphthalene are the highest among the three PAHs. At an OA concentration of 1 µg m^{-3}, the estimated SOA yield of naphthalene is 4.2 %, of 2-methylnaphthalene it is 4 % and of 1-methylnaphthalene it is 6.4 %. At higher OA levels of 10 µg m^{-3}, the estimated SOA yields are respectively 19.3 %, 21.2 % and 24.5 %. Under low-NO$_x$ conditions, at OA concentration of 1 µg m^{-3}, the SOA yield of 2-methylnaphthalene is 5.7 %, and for both naphthalene and 1-methylnaphthalene it is 4 %. Under the same conditions and at OA of 10 µg m^{-3}, 2-methylnaphthalene is estimated to have a yield of 31.4 %, 1-methylnaphthalene 23 % and naphthalene 22.6 %.

Our parametrization suggests that under low-NO$_x$ conditions, the yields of 2-methylnaphthalene are higher than those of naphthalene and 1-methylnaphthalene. Due to the variability of experimental methods used, there has been a lack of consensus among experimental studies about which of the three studied PAHs has the highest and the lowest SOA yields. For example, we estimated that under low-NO$_x$ conditions, the SOA yields of 1-methylnaphthalene are lower than those of 2-methylnaphthalene. This is in line with observations made by Chan et al. (2009) and Kleindienst et al. (2012), but at the same time it contradicts the results of Shakya and Griffin (2010) and Chen et al. (2016), who propose that the yields of 1-methylnaphthalene are higher than those of 2-methylnaphthalene. Since all three PAHs are lumped into the same species, PAH1, these experimental discrepancies have little effect on our final yield parametrization.

For both low- and high-NO$_x$ conditions, the VBS parametrization of the lumped PAHs can be found in Table 3, and the resultant SOA yields as a function of OA are shown in Fig. 10. Under high-NO$_x$ conditions at organic aerosol concentration of 1 µg m^{-3}, the estimated yield of PAH1 is 3.8 %,

and at organic aerosol concentration 10 µg m^{-3} it is 19 %. For PAH2, the estimated yields are 3.8 % and 21 % respectively. Under low-NO$_x$ conditions for PAH1 and PAH2, at the organic aerosol concentration of 1 µg m^{-3}, the estimated yields are 4.6 % and 5.7 %, and at organic aerosol concentrations of 10 µg m^{-3}, they are respectively 25 % and 31.4 %. For both lumped species, the estimated yields under low-NO$_x$ conditions are higher than those under high-NO$_x$ conditions. This is consistent with the observations which suggest that under high-NO$_x$ conditions the PAHs' reaction with the OH radical is dominated by the fragmentation route, which leads to higher-volatility products (Chan et al., 2009; Shakya and Griffin, 2010; Kleindienst et al., 2012).

3.2.3 Aromatic yields

The estimated parameters for ARO3 are shown in Table 3. The estimated yields of ARO3 are shown as a function of organic aerosol concentration in Fig. 11, together with the yields of ARO2, the lumped species which the mass-based yields of ARO3 were based upon. At the organic aerosol concentration of 1 µg m^{-3}, under high-NO$_x$ conditions the estimated mass fraction of ARO3 is 8.7 %, and under low-NO$_x$ conditions it is 17.2 %. At organic aerosol concentration of 10 µg m^{-3}, under high-NO$_x$ conditions the estimated aerosol mass fraction of ARO3 is 10.4 %, and under low-NO$_x$ conditions it is 20.6 %. Like in the case of the new lumped PAHs, the new aromatic species has higher SOA yields under high-NO$_x$ than under low-NO$_x$ conditions. This is consistent with experimental observations that have shown that due to the formation of the alkoxyl radical, which decomposes more easily in the atmosphere, SOA formation from aromatics under high-NO$_x$ conditions is less effective (Ng et al., 2007).
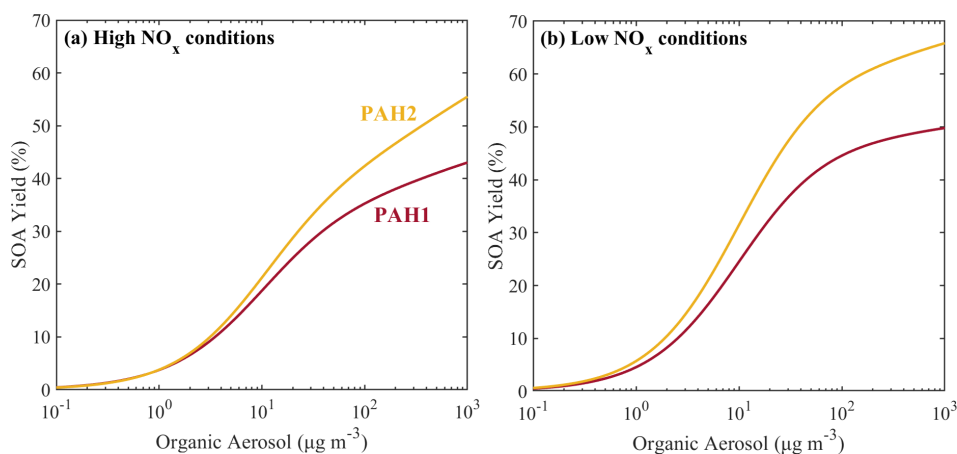
Figure 10. Estimated aerosol mass fractions of the new lumped PAH species under **(a)** high-NO$_x$ and **(b)** low-NO$_x$ conditions. The yield curves are generated using the mass-based yields of Table 3.

Table 3. Aerosol mass-based yields for the new lumped species in the IVOC range using a five-product basis set with saturation concentrations of 0.1, 1, 10, 100 and 10^3 µg m^{-3} at 298 K.

Lumped species	Aerosol mass-based yields				
	0.1 µg m^{-3}	1 µg m^{-3}	10 µg m^{-3}	100 µg m^{-3}	10^3 µg m^{-3}
High-NO$_x$ parametrization					
ALK6	0.038	0.035	0.03	0.062	0.309
ALK7	0.025	0.117	0.401	0.103	0.052
ALK8	0.074	0.029	0.622	0.148	0
ALK9	0.077	0.024	0.629	0.151	0
ARO3	0	0.001	0.156	0.24	0.348
PAH1	0	0.011	0.346	0.038	0.083
PAH2	0	0	0.407	0.077	0.163
Low-NO$_x$ parametrization					
ALK6	0.038	0.035	0.03	0.062	0.309
ALK7	0.025	0.117	0.401	0.103	0.052
ALK8	0.074	0.029	0.622	0.148	0
ALK9	0.077	0.024	0.629	0.151	0
ARO3	0	0.06	0.24	0.3	0.42
PAH1	0	0.003	0.484	0	0.032
PAH2	0	0	0.627	0	0.074

4 Conclusions

A new approach for simulating IVOC chemistry and SOA production in CTMs is developed. IVOCs are treated as lumped species, similar to the larger VOCs. The new lumping method takes into account both the complex chemistry and the organic aerosol formation potential of the IVOC lumped species. One of the benefits of our approach is that the new lumped scheme is consistent with the structure of the SAPRC gas-phase chemical mechanism and therefore can be easily integrated into models that utilize this mechanism. At the same time, it can also be used in other gas-phase chemistry schemes. Our lumping approach can be viewed as an exten-

sion of the lumping scheme proposed by Lu et al. (2020), further separating the individual compounds based on their specific chemical structure and reactivity. This additional separation also allows us to quantify the contribution of specific compounds to the formed SOA-iv, as opposed to the limited information available from previous efforts.

Our estimated IVOC emissions from diesel and gasoline vehicles in Europe are 8 times higher compared to the IVOC emissions previously used, which were equal to 1.5 times the primary OA emissions. Cyclic alkanes have the highest emissions (63 % of the total), followed by branched alkanes (15 % of the total) and unspeciated aromatic compounds (13 % of
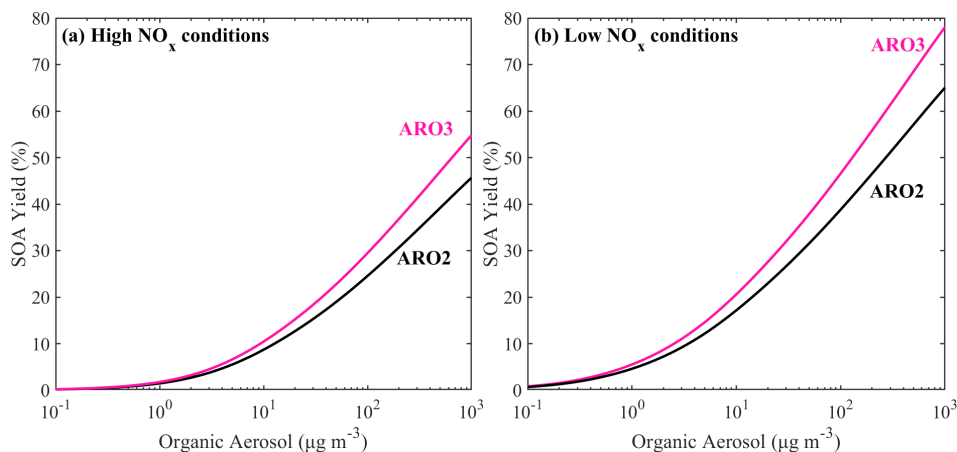
Figure 11. Estimated aerosol yields for the new aromatic species (ARO3) and the existing ARO2 species under **(a)** high-NO$_x$ and **(b)** low-NO$_x$ conditions.

the total). These compounds are mostly unspeciated and appear usually in the mass spectrometry–gas chromatography measurements as an unresolved complex mixture.

The estimated SOA yields of IVOCs are significantly higher than those of the VOCs currently in the model. Specifically, under high-NO$_x$ conditions at organic aerosol concentration of $10 \, \mu g \, m^{-3}$, the aerosol mass fractions of the new lumped alkanes (ALK6–ALK9) are on average 6.4 times higher than those of ALK5, and the aerosol mass fractions of the new lumped PAHs (PAH1 and PAH2) and ARO3 are on average 9.6 times higher than those of ARO2. Since the estimates of the SOA yields of the new lumped species are based on data for only nine individual IVOCs, there is significant uncertainty in these values. Smog chamber experiments with the IVOCs that are lumped into the new lumped species are necessary in order to improve the estimates of the yields.

A first application of the new approach in PMCAMx-iv, the results of which will be presented in a subsequent publication, will provide a clearer perspective on which individual IVOCs experimental studies should be focusing on. The sensitivity of the predicted SOA-iv from transportation to our major assumptions will also be examined.

Author contributions. SEIM and SNP designed the research. SEIM developed the lumping scheme, prepared the source-specific IVOC emissions over the European domain, and designed the SOA

parametrization for the new IVOC lumped species. SEIM wrote the paper with input from SNP.

References

ACEA: Vehicles in use – Europe 2017, ACEA Report, https://www.acea.auto/uploads/statistic_documents/ACEA_Report_Vehicles_in_use-Europe_2017.pdf (last access: 18 October 2022), 2017.

Akherati, A., Cappa, C. D., Kleeman, M. J., Docherty, K. S., Jimenez, J. L., Griffith, S. M., Dusanter, S., Stevens, P. S., and Jathar, S. H.: Simulating secondary organic aerosol in a regional air quality model using the statistical oxidation model – Part 3: Assessing the influence of semi-volatile and intermediate-volatility organic compounds and NO$_x$, Atmos. Chem. Phys., 19, 4561–4594, https://doi.org/10.5194/acp-19-4561-2019, 2019.

Ananthula, R., Yamada, T., and Taylor, P. H.: Kinetics of OH radical reaction with anthracene and anthracene-d10, J. Phys. Chem. A, 110, 3559–3566, https://doi.org/10.1021/jp054301c, 2006.

Atkinson, R. and Arey, J.: Atmospheric degradation of volatile organic compounds, Chem. Rev., 103, 4605–4638, https://doi.org/10.1021/cr0206420, 2003.

Aumont, B., Valorso, R., Mouchel-Vallon, C., Camredon, M., Lee-Taylor, J., and Madronich, S.: Modeling SOA formation from the oxidation of intermediate volatility n-alkanes, Atmos. Chem. Phys., 12, 7577–7589, https://doi.org/10.5194/acp-12-7577-2012, 2012.

Aumont, B., Camredon, M., Mouchel-Vallon, C., La, S., Ouzebidour, F., Valorso, R., Lee-Taylor, J., and Madronich, S.: Modeling the influence of alkane molecular structure on secondary organic aerosol formation, Faraday Discuss., 165, 105–122, https://doi.org/10.1039/C3FD00029J, 2013.

Barsanti, K. C., Carlton, A. G., and Chung, S. H.: Analyzing experimental data and model parameters: implications for predictions of SOA using chemical transport models, Atmos. Chem. Phys., 13, 12073–12088, https://doi.org/10.5194/acp-13-12073-2013, 2013.

Carter, W. P. L.: Development of the SAPRC-07 chemical mechanism, Atmos. Environ., 44, 5324–5335, https://doi.org/10.1016/j.atmosenv.2010.01.026, 2010.

Chambers, M. and Schmitt, R.: Diesel-powered passenger cars and light trucks, US DOT, BTS, Fact Sheet, https://www.bts.gov/sites/bts.dot.gov/files/legacy/DieselFactSheet.pdf (last access: 16 October 2022), 2015.

Chan, A. W. H., Kautzman, K. E., Chhabra, P. S., Surratt, J. D., Chan, M. N., Crounse, J. D., Kürten, A., Wennberg, P. O., Flagan, R. C., and Seinfeld, J. H.: Secondary organic aerosol formation from photooxidation of naphthalene and alkylnaphthalenes: implications for oxidation of intermediate volatility organic compounds (IVOCs), Atmos. Chem. Phys., 9, 3049–3060, https://doi.org/10.5194/acp-9-3049-2009, 2009.

Chen, C.-L., Kacarab, M., Tang, P., and Cocker, D. R.: SOA formation from naphthalene, 1-methylnaphthalene, and 2-methylnaphthalene photooxidation, Atmos. Environ., 131, 424–433, https://doi.org/10.1016/j.atmosenv.2016.02.007, 2016.

Ciarelli, G., El Haddad, I., Bruns, E., Aksoyoglu, S., Möhler, O., Baltensperger, U., and Prévôt, A. S. H.: Constraining a hybrid volatility basis-set model for aging of wood-burning emissions using smog chamber experiments: a box-model study based on the VBS scheme of the CAMx model (v5.40), Geosci. Model Dev., 10, 2303–2320, https://doi.org/10.5194/gmd-10-2303-2017, 2017.

Cross, E. S., Sappok, A. G., Wong, V. W., and Kroll, J. H.: Load-dependent emission factors and chemical characteristics of IVOCs from a medium-duty diesel engine, Environ. Sci. Technol., 49, 13483–13491, https://doi.org/10.1021/acs.est.5b03954, 2015.

Docherty, K. S., Yaga, R., Preston, W. T., Jaoui, M., Reidel, T. P., Offenberg, J. H., Kleindienst, T. E., and Lewandowski, M.: Relative contributions of selected multigeneration products to chamber SOA formed from photooxidation of a range (C10–C17) of n-alkanes under high NO_x conditions, Atmos. Environ., 244, 117976, https://doi.org/10.1016/j.atmosenv.2020.117976, 2021.

Donahue, N. M., Robinson, A. L., Stanier, C. O., and Pandis, S. N.: Coupled partitioning, dilution, and chemical aging of semivolatile organics, Environ. Sci. Technol., 40, 2635–2643, https://doi.org/10.1021/es052297c, 2006.

Drozd, G. T., Zhao, Y., Saliba, G., Frodin, B., Maddox, C., Oliver Chang, M. C., Maldonado, H., Sardar, S., Weber, R. J., Robinson, A. L., and Goldstein, A. H.: Detailed speciation of intermediate volatility and semivolatile organic compound emissions from gasoline vehicles: effects of cold-starts and implications for secondary organic aerosol formation, Environ. Sci. Technol., 53, 1706–1714, https://doi.org/10.1021/acs.est.8b05600, 2019.

Environ: User's Guide to the Comprehensive Air Quality Model with Extensions (CAMx), Version 6.00, Report prepared by ENVIRON Int. Corp., Novato, CA, 2013.

Fang, H., Huang, X., Zhang, Y., Pei, C., Huang, Z., Wang, Y., Chen, Y., Yan, J., Zeng, J., Xiao, S., Luo, S., Li, S., Wang, J., Zhu, M., Fu, X., Wu, Z., Zhang, R., Song, W., Zhang, G., Hu, W., Tang, M., Ding, X., Bi, X., and Wang, X.: Measurement report: Emissions of intermediate-volatility organic compounds from vehicles under real-world driving conditions in an urban tunnel, Atmos. Chem. Phys., 21, 10005-10013, https://doi.org/10.5194/acp-21-10005-2021, 2021.

Gentner, D., Isaacman, G., Worton, D., Chan, A., Dallmann, T., Davis, L., Liu, S., Day, D., Russell, L., Wilson, K., Weber, R., Guha, A., Harley, R., and Goldstein, A.: Elucidating secondary organic aerosol from diesel and gasoline vehicles through detailed characterization of organic carbon emissions, P. Natl. Acad. Sci. USA, 109, 18318–18323, https://doi.org/10.1073/pnas.1212272109, 2012.

Giani, P., Balzarini, A., Pirovano, G., Gilardoni, S., Paglione, M., Colombi, C., Gianelle, V. L., Belis, C. A., Poluzzi, V., and Lonati, G.: Influence of semi- and intermediate-volatile organic compounds (S/IVOC) parameterizations, volatility distributions and aging schemes on organic aerosol modelling in winter conditions, Atmos. Environ., 213, 11–24, https://doi.org/10.1016/j.atmosenv.2019.05.061, 2019.

Gordon, T. D., Presto, A. A., May, A. A., Nguyen, N. T., Lipsky, E. M., Donahue, N. M., Gutierrez, A., Zhang, M., Maddox, C., Rieger, P., Chattopadhyay, S., Maldonado, H., Maricq, M. M., and Robinson, A. L.: Secondary organic aerosol formation exceeds primary particulate matter emissions for light-duty gasoline vehicles, Atmos. Chem. Phys., 14, 4661–4678, https://doi.org/10.5194/acp-14-4661-2014, 2014.

Hatch, L. E., Yokelson, R. J., Stockwell, C. E., Veres, P. R., Simpson, I. J., Blake, D. R., Orlando, J. J., and Barsanti, K. C.: Multi-instrument comparison and compilation of non-methane organic gas emissions from biomass burning and implications for smoke-derived secondary organic aerosol precursors, Atmos. Chem. Phys., 17, 1471–1489, https://doi.org/10.5194/acp-17-1471-2017, 2017.

Huang, C., Hu, Q., Li, Y., Tian, J., Ma, Y., Zhao, Y., Feng, J., An, J., Qiao, L., Wang, H., Jing, S. A., Huang, D., Lou, S., Zhou, M., Zhu, S., Tao, S., and Li, L.: Intermediate volatility organic compound emissions from a large cargo vessel operated under real-world conditions, Environ. Sci. Technol., 52, 12934–12942, https://doi.org/10.1021/acs.est.8b04418, 2018.

Huang, L., Wang, Q., Wang, Y., Emery, C., Zhu, A., Zhu, Y., Yin, S., Yarwood, G., Zhang, K., and Li, L.: Simulation of secondary organic aerosol over the Yangtze River Delta region: The impacts from the emissions of intermediate volatility organic compounds

and the SOA modeling framework, Atmos. Environ., 246, 118079, https://doi.org/10.1016/j.atmosenv.2020.118079, 2021.

Jathar, S. H., Miracolo, M. A., Tkacik, D. S., Donahue, N. M., Adams, P. J., and Robinson, A. L.: Secondary organic aerosol formation from photo-oxidation of unburned fuel: experimental results and implications for aerosol formation from combustion emissions, Environ. Sci. Technol., 47, 12886–12893, https://doi.org/10.1021/es403445q, 2013.

Jathar, S. H., Gordon, T. D., Hennigan, C. J., Pye, H. O. T., Pouliot, G., Adams, P. J., Donahue, N. M., and Robinson, A. L.: Unspeciated organic emissions from combustion sources and their influence on the secondary organic aerosol budget in the United States, P. Natl. Acad. Sci. USA, 111, 10473, https://doi.org/10.1073/pnas.1323740111, 2014.

Jathar, S. H., Friedman, B., Galang, A. A., Link, M. F., Brophy, P., Volckens, J., Eluri, S., and Farmer, D. K.: Linking load, fuel, and emission controls to photochemical production of secondary organic aerosol from a diesel engine, Environ. Sci. Technol., 51, 1377–1386, https://doi.org/10.1021/acs.est.6b04602, 2017.

Kameda, T., Inazu, K., Asano, K., Murota, M., Takenaka, N., Sadanaga, Y., Hisamatsu, Y., and Bandow, H.: Prediction of rate constants for the gas phase reactions of triphenylene with OH and NO_3 radicals using a relative rate method in CCl4 liquid phase-system, Chemosphere, 90, 766–771, https://doi.org/10.1016/j.chemosphere.2012.09.071, 2013.

Kleindienst, T. E., Jaoui, M., Lewandowski, M., Offenberg, J. H., and Docherty, K. S.: The formation of SOA and chemical tracer compounds from the photooxidation of naphthalene and its methyl analogs in the presence and absence of nitrogen oxides, Atmos. Chem. Phys., 12, 8711–8726, https://doi.org/10.5194/acp-12-8711-2012, 2012.

Koo, B., Knipping, E., and Yarwood, G.: 1.5-Dimensional volatility basis set approach for modeling organic aerosol in CAMx and CMAQ, Atmos. Environ, 95, 158–164, https://doi.org/10.1016/j.atmosenv.2014.06.031, 2014.

Kwok, E. S. C. and Atkinson, R.: Estimation of hydroxyl radical reaction rate constants for gas-phase organic compounds using a structure-reactivity relationship: An update, Atmos. Environ, 29, 1685–1695, https://doi.org/10.1016/1352-2310(95)00069-B, 1995.

Kwok, E. S. C., Atkinson, R., and Arey, J.: Kinetics of the gas-phase reactions of indan, indene, fluorene, and 9,10-dihydroanthracene with OH radicals, NO_3 radicals, and O_3, Int. J. Chem. Kinet., 29, 299–309, https://doi.org/10.1002/(SICI)1097-4601(1997)29:4<299::AID-KIN9>3.0.CO;2-P, 1997.

Lee, W., Stevens, P. S., and Hites, R. A.: Rate constants for the gas-phase reactions of methylphenanthrenes with oh as a function of temperature, J. Phys. Chem. A, 107, 6603–6608, https://doi.org/10.1021/jp034159k, 2003.

Li, W., Li, L., Chen, C.-L., Kacarab, M., Peng, W., Price, D., Xu, J., and Cocker, D. R.: Potential of select intermediate-volatility organic compounds and consumer products for secondary organic aerosol and ozone formation under relevant urban conditions, Atmos. Environ, 178, 109–117, https://doi.org/10.1016/j.atmosenv.2017.12.019, 2018.

Li, Y., Ren, B., Qiao, Z., Zhu, J., Wang, H., Zhou, M., Qiao, L., Lou, S., Jing, S., Huang, C., Tao, S., Rao, P., and Li, J.: Characteristics of atmospheric intermediate volatility organic compounds (IVOCs) in winter and summer under different air pollution levels, Atmos. Environ, 210, 58–65, https://doi.org/10.1016/j.atmosenv.2019.04.041, 2019.

Lim, Y. B. and Ziemann, P. J.: Effects of molecular structure on aerosol yields from OH radical-initiated reactions of linear, branched, and cyclic alkanes in the presence of NO_x, Environ. Sci. Technol., 43, 2328–2334, https://doi.org/10.1021/es803389s, 2009.

Lou, H., Hao, Y., Zhang, W., Su, P., Zhang, F., Chen, Y., Feng, D., and Li, Y.: Emission of intermediate volatility organic compounds from a ship main engine burning heavy fuel oil, J. Environ. Sci., 84, 197–204, https://doi.org/10.1016/j.jes.2019.04.029, 2019.

Lu, Q., Zhao, Y., and Robinson, A. L.: Comprehensive organic emission profiles for gasoline, diesel, and gas-turbine engines including intermediate and semi-volatile organic compound emissions, Atmos. Chem. Phys., 18, 17637–17654, https://doi.org/10.5194/acp-18-17637-2018, 2018.

Lu, Q., Murphy, B. N., Qin, M., Adams, P. J., Zhao, Y., Pye, H. O. T., Efstathiou, C., Allen, C., and Robinson, A. L.: Simulation of organic aerosol formation during the CalNex study: updated mobile emissions and secondary organic aerosol parameterization for intermediate-volatility organic compounds, Atmos. Chem. Phys., 20, 4313–4332, https://doi.org/10.5194/acp-20-4313-2020, 2020.

Manavi, S. E. I. and Pandis, S. N.: Code and data: A lumped species approach for the simulation of secondary organic aerosol production from intermediate volatility organic compounds (IVOCs): Application to road transport in PMCAMx-iv (v1.0), Geoscientific Model Development, Zenodo [data set and code], https://doi.org/10.5281/zenodo.6515734, 2022.

Murphy, B. N. and Pandis, S. N.: Simulating the formation of semivolatile primary and secondary organic aerosol in a regional chemical transport model, Environ. Sci. Technol., 43, 4722–4728, https://doi.org/10.1021/es803168a, 2009.

Nannoolal, Y., Rarey, J., and Ramjugernath, D.: Estimation of pure component properties: Part 3. Estimation of the vapor pressure of non-electrolyte organic compounds via group contributions and group interactions, Fluid Phase Equilibria, 269, 117–133, https://doi.org/10.1016/j.fluid.2008.04.020, 2008.

Ng, N. L., Kroll, J. H., Chan, A. W. H., Chhabra, P. S., Flagan, R. C., and Seinfeld, J. H.: Secondary organic aerosol formation from m-xylene, toluene, and benzene, Atmos. Chem. Phys., 7, 3909–3922, https://doi.org/10.5194/acp-7-3909-2007, 2007.

Ots, R., Vieno, M., Allan, J. D., Reis, S., Nemitz, E., Young, D. E., Coe, H., Di Marco, C., Detournay, A., Mackenzie, I. A., Green, D. C., and Heal, M. R.: Model simulations of cooking organic aerosol (COA) over the UK using estimates of emissions based on measurements at two sites in London, Atmos. Chem. Phys., 16, 13773–13789, https://doi.org/10.5194/acp-16-13773-2016, 2016.

Pennington, E. A., Seltzer, K. M., Murphy, B. N., Qin, M., Seinfeld, J. H., and Pye, H. O. T.: Modeling secondary organic aerosol formation from volatile chemical products, Atmos. Chem. Phys., 21, 18247–18261, https://doi.org/10.5194/acp-21-18247-2021, 2021.

Phousongphouang, P. T. and Arey, J.: Rate constants for the gas-phase reactions of a series of alkylnaphthalenes with the OH radical, Environ. Sci. Technol., 36, 1947–1952, https://doi.org/10.1021/es011434c, 2002.

Presto, A. A., Miracolo, M. A., Donahue, N. M., and Robinson, A. L.: secondary organic aerosol formation from high-NO_x photooxidation of low volatility precursors: n-alkanes, Environ. Sci. Technol., 44, 2029–2034, https://doi.org/10.1021/es903712r, 2010.

Pye, H. O. T. and Seinfeld, J. H.: A global perspective on aerosol from low-volatility organic compounds, Atmos. Chem. Phys., 10, 4377–4401, https://doi.org/10.5194/acp-10-4377-2010, 2010.

Qi, L., Liu, H., Shen, X. E., Fu, M., Huang, F., Man, H., Deng, F., Shaikh, A. A., Wang, X., Dong, R., Song, C., and He, K.: Intermediate-volatility organic compound emissions from nonroad construction machinery under different operation modes, Environ. Sci. Technol., 53, 13832–13840, https://doi.org/10.1021/acs.est.9b01316, 2019.

Qian, Z., Chen, Y., Liu, Z., Han, Y., Zhang, Y., Feng, Y., Shang, Y., Guo, H., Li, Q., Shen, G., Chen, J., and Tao, S.: Intermediate volatile organic compound emissions from residential solid fuel combustion based on field measurements in rural China, Environ. Sci. Technol., 55, 5689–5700, https://doi.org/10.1021/acs.est.0c07908, 2021.

Qin, M., Murphy, B. N., Isaacs, K. K., McDonald, B. C., Lu, Q., McKeen, S. A., Koval, L., Robinson, A. L., Efstathiou, C., Allen, C., and Pye, H. O. T.: Criteria pollutant impacts of volatile chemical products informed by near-field modelling, Nat. Sustain., 4, 129–137, 10.1038/s41893-020-00614-1, 2021.

Reisen, F. and Arey, J.: Reactions of hydroxyl radicals and ozone with acenaphthene and acenaphthylene, Environ. Sci. Technol., 36, 4302–4311, https://doi.org/10.1021/es025761b, 2002.

Robinson, A. L., Donahue, N. M., Shrivastava, M. K., Weitkamp, E. A., Sage, A. M., Grieshop, A. P., Lane, T. E., Pierce, J. R., and Pandis, S. N.: rethinking organic aerosols: semivolatile emissions and photochemical aging, Science, 315, 1259, https://doi.org/10.1126/science.1133061, 2007.

Schauer, J. J., Kleeman, M. J., Cass, G. R., and Simoneit, B. R. T.: Measurement of emissions from air pollution sources. 2. C1 through C30 organic compounds from medium duty diesel trucks, Environ. Sci. Technol., 33, 1578–1587, https://doi.org/10.1021/es980081n, 1999.

Schauer, J. J., Kleeman, M. J., Cass, G. R., and Simoneit, B. R. T.: Measurement of emissions from air pollution sources. 3. C1−C29 organic compounds from fireplace combustion of wood, Environ. Sci. Technol., 35, 1716–1728, https://doi.org/10.1021/es001331e, 2001.

Seltzer, K. M., Pennington, E., Rao, V., Murphy, B. N., Strum, M., Isaacs, K. K., and Pye, H. O. T.: Reactive organic carbon emissions from volatile chemical products, Atmos. Chem. Phys., 21, 5079–5100, https://doi.org/10.5194/acp-21-5079-2021, 2021.

Shakya, K. M. and Griffin, R. J.: Secondary organic aerosol from photooxidation of polycyclic aromatic hydrocarbons, Environ. Sci. Technol., 44, 8134–8139, https://doi.org/10.1021/es1019417, 2010.

Stanier, C. O., Donahue, N., and Pandis, S. N.: Parameterization of secondary organic aerosol mass fractions from smog chamber data, Atmos. Environ, 42, 2276–2299, https://doi.org/10.1016/j.atmosenv.2007.12.042, 2008.

Su, P., Hao, Y., Qian, Z., Zhang, W., Chen, J., Zhang, F., Yin, F., Feng, D., Chen, Y., and Li, Y.: Emissions of intermediate volatility organic compound from waste cooking oil biodiesel and marine gas oil on a ship auxiliary engine, J. Environ. Sci., 91, 262–270, https://doi.org/10.1016/j.jes.2020.01.008, 2020.

Tang, R., Lu, Q., Guo, S., Wang, H., Song, K., Yu, Y., Tan, R., Liu, K., Shen, R., Chen, S., Zeng, L., Jorga, S. D., Zhang, Z., Zhang, W., Shuai, S., and Robinson, A. L.: Measurement report: Distinct emissions and volatility distribution of intermediate-volatility organic compounds from on-road Chinese gasoline vehicles: implication of high secondary organic aerosol formation potential, Atmos. Chem. Phys., 21, 2569–2583, https://doi.org/10.5194/acp-21-2569-2021, 2021.

Tkacik, D. S., Presto, A. A., Donahue, N. M., and Robinson, A. L.: Secondary organic aerosol formation from intermediate-volatility organic compounds: cyclic, linear, and branched alkanes, Environ. Sci. Technol., 46, 8773–8781, https://doi.org/10.1021/es301112c, 2012.

Tsimpidi, A. P., Karydis, V. A., Zavala, M., Lei, W., Molina, L., Ulbrich, I. M., Jimenez, J. L., and Pandis, S. N.: Evaluation of the volatility basis-set approach for the simulation of organic aerosol formation in the Mexico City metropolitan area, Atmos. Chem. Phys., 10, 525–546, https://doi.org/10.5194/acp-10-525-2010, 2010.

Visschedijk, A. J. H., Zandveld, P., and Denier van der Gon, H. A. C.: A high resolution gridded European emission database for the EU integrated project GEMS, TNO Report 2007 A-R0233/B: Organization for Applied Scientific Research, the Netherlands, 2007.

Woody, M. C., West, J. J., Jathar, S. H., Robinson, A. L., and Arunachalam, S.: Estimates of non-traditional secondary organic aerosols from aircraft SVOC and IVOC emissions using CMAQ, Atmos. Chem. Phys., 15, 6929–6942, https://doi.org/10.5194/acp-15-6929-2015, 2015.

Woody, M. C., Wong, H. W., West, J. J., and Arunachalam, S.: Multiscale predictions of aviation-attributable $PM_{2.5}$ for U.S. airports modelled using CMAQ with plume-in-grid and an aircraft-specific 1-D emission model, Atmos. Environ., 147, 384–394, https://doi.org/10.1016/j.atmosenv.2016.10.016, 2016.

Zhao, Y., Hennigan, C. J., May, A. A., Tkacik, D. S., de Gouw, J. A., Gilman, J. B., Kuster, W. C., Borbon, A., and Robinson, A. L.: Intermediate-volatility organic compounds: a large source of secondary organic aerosol, Environ. Sci. Technol., 48, 13743–13750, https://doi.org/10.1021/es5035188, 2014.

Zhao, Y., Nguyen, N. T., Presto, A. A., Hennigan, C. J., May, A. A., and Robinson, A. L.: Intermediate volatility organic compound emissions from on-road diesel vehicles: chemical composition, emission factors, and estimated secondary organic aerosol production, Environ. Sci. Technol., 49, 11516–11526, https://doi.org/10.1021/acs.est.5b02841, 2015.

Zhao, Y., Nguyen, N. T., Presto, A. A., Hennigan, C. J., May, A. A., and Robinson, A. L.: Intermediate volatility organic compound emissions from on-road gasoline vehicles and small off-road gasoline engines, Environ. Sci. Technol., 50, 4554–4563, https://doi.org/10.1021/acs.est.5b06247, 2016.